Why slot and hybrid plasmonic waveguides are ideal candidates for sensing applications?

N. L. KAZANSKIY[a,b], A. KAŹMIERCZAK[c], M. A. BUTT[a,c,*]
[a]Samara National Research University, 34 Moskovkoye Shosse, Samara 443086, Russia
[b]Institute of RAS-Branch of the FSRC "Crystallography and Photonics" RAS, 151 Molodogvardeiskaya, Samara 443001, Russia
[c]Warsaw University of Technology, Institute of Microelectronics and Optoelectronics, Koszykowa 75, 00-662 Warszawa, Poland

In this paper, the modal characteristics of silicon-based optical waveguides (hereafter represented as WGs) such as ridge, rib, slot and the hybrid plasmonic WGs are discussed. For sensing applications, the geometric parameters of the WGs are optimized to evaluate the mode sensitivity (S_{mode}) and evanescent field ratio (EFR). For highly sensitive devices, these two parameters should be as high as possible to facilitate strong light-matter interaction. The analysis is performed via the finite element method (FEM) which demonstrate that EFR and S_{mode} follow the following order: Hybrid WG ≥ Slot WG > Ridge WG @ TE mode > Rib WG @ TE-mode > Ridge WG @ TM mode > Rib WG @ TM mode. Furthermore, refractive index sensor established on a ridge, slot and hybrid plasmonic WGs are studied. The numerical calculations have revealed that the best sensitivity of 167 nm/RIU, 233.3 nm/RIU and 333.3 nm/RIU is delivered by ring resonator designs constructed on ridge, slot and the hybrid plasmonic WG, respectively. We believe that these findings are quite beneficial to have a detailed analysis of different WG types to make a judicious selection of optical WG structure for sensing applications.

1. Introduction

Silicon is not only a highly attractive platform for integrated electronics but also transparent in the infrared (IR) region which supports low-loss optical waveguiding [1, 2]. The integration of photonics with electronics on a single-chip enables several technologies such as light sources, light guiding, light modulation, and light detection. In the silicon on insulator (SOI) platform, the silicon (hereafter represented as Si) WG layer acts as a core on top of a buried oxide (SiO_2) which is used as cladding. The refractive index of the Si and the SiO_2 are 3.476 and 1.444 for 1550 nm wavelength, respectively [3]. This WG system is compatible with complementary metal-oxide-semiconductor (CMOS), high index contrast WG which permits the realization of smaller bends, i.e., miniaturized devices. Si is proficient in realizing multi functionalities on a single chip due to the high integration density. Miniaturized optical elements increase the number of chips per wafer, which significantly lowers the cost of a single-chip.

The main shortcoming is that the Si WGs are extremely intolerant to fabrication flaws: the optical losses are increased due to sidewall roughness of the WG and also induces phase error. Furthermore, the Si WGs are robustly birefringent, have considerable temperature dependence, and the chip to fiber coupling loss is significantly high. Although many different types of Si channel WGs are proposed [4-6], our focus will be on the most widely used photonic WGs such as ridge, rib, slot and hybrid plasmonic suitable for different applications such as lasers [6, 7], amplifiers [8], modulators [9], splitters [10, 11] and switches [12], sensors [13,14] and couplers [15], among others.

The geometry of the WG should support fundamental mode, if not the higher-order modes couple into the neighbour regions that could add to the propagation loss. Moreover, higher-order modes are susceptible to a dispersion that deforms optical pulses while propagating in the WG. Therefore, the generalized conditions for fundamental modes are vital [16]. Even though these fundamental WG schemes are customary. Recently there are several attempts to transform the basic geometry of the WG to confine the light in a low index medium. The objective depends on confining the light inside the low refractive index region because of E-field discontinuity at the interface between the high index and low index mediums. Slot and HPWG attracted vast research activities in sensors, lasers, and electro-optic modulators [17, 18] areas due to their better field manipulation capabilities.

In this paper, we investigated the mode sensitivity and evanescent field ratio of ridge, rib, slot and hybrid

plasmonic (HP) WGs. The evaluation of the effective refractive index (n_{eff}) is very important while creating the optical system because it manages the propagation constant of the optical mode. The dispersion is a limiting factor in high-speed communication, that's why it is critical to evaluate. The Electric field distribution and n_{eff} of Si WGs are analyzed via a 2D finite element method (FEM) in COMSOL Multiphysics 5.1. The EM-wave frequency domain (emw) is selected as the physics interface and the modal analysis was added to the study. While, the propagation loss, sensitivity and evanescent field ratio are studied with the help of the 3D-FEM model in the above-mentioned module.

2. Optical WG geometries

In this section, four major optical WGs based on Si photonics are discussed namely: Ridge, rib, slot and hybrid plasmonic WG.

1) The ridge WG is composed of Si core embedded on a silica substrate as shown in Fig. 1a, where W_{Si} and H_{Si} are the width and height of the core, respectively. The single-mode condition is a crucial step in the realization of functional devices, therefore the Si core should be design in such a way that it can satisfy the single-mode condition [16, 19]. The principal requirement of the ridge WG is the guiding of a single TE_{00} and TM_{00} mode.

2) The rib WG can be seen as a special case of ridge WG where the Si layer is not completely etched. The guiding layer mainly consists of the slab with a strip placed onto it. As shown in Fig. 1b, H_{Slab} is the slab height, W_{Si} is the strip width and $H_{Si} + H_{slab}$ is the total rib height. SOI WGs with dimensions bigger than a few nanometers support multiple modes which makes them highly unattractive to be integrated in photonic integrated circuits. However, there are some attempts to develop monomodal large rib WGs [20]. An advantage of using large rib WG is that they can relatively facilitate the low-loss coupling to the optical fiber.

3) The slot WGs are the structure that can confine light in a low-index material between two high index rail WGs. The height and width of the silicon rail are denoted as H_{Si} and W_{Si}, respectively. While the gap between the rails is represented as g. The slot WG structure is shown in Fig. 1c. The quasi-TE polarized light experiences high discontinuity at the interface between a high and a low refractive index material, which is responsible for providing a prominent intensity of light in the low index slot [21-23].

4) Hybrid plasmonic WGs (HPWGs) has gathered substantial attention as they can provide both subwavelength confinement and extended propagation lengths [24]. These WGs structures are composed of a thin layer of low refractive index material (SiO_2) inserted between the metal layer (Au or Ag) and a higher index dielectric layer (Si) as shown in Fig. 1d. Where H_{Si}, W_{Si}, g, W_{Au} signifies the layer thickness of the Si core, the width of

the Si core, the width of the nano-slot and the width of the Au layer, respectively. Theoretical studies have shown that a low index layer can support a low loss mode whose propagation length robustly rely on its thickness [25]. The detailed solution of hybrid mode supported by HPWG is presented in our previous work [26]. The working mechanism of the HPWG can be explained using the mode-coupling theory [27]. The dielectric WG mode is generally confined in the Si core while the surface plasmons (SPs) are supported by the metal surface. When these two WG configurations are brought close to each other, the dielectric WG mode supported by Si ridge couples to the SP mode supported by the metal surface. Consequently, the light is transferred to the gap between the metal and the high index medium because of the mode coupling.
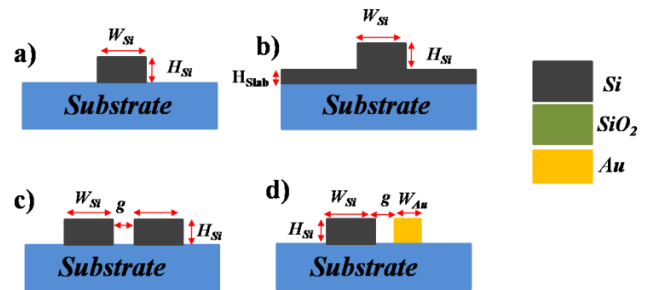

Fig. 1. Graphical illustration of Si WGs, a) Ridge WG, b) Rib WG, c) Slot WG, d) HPWG (color online)

The E-field intensity arrangement of TE and TM modes in the abovementioned WGs at 1550 nm is shown in Fig. 2. In the case of ridge and rib WGs, the main part of the mode power is concentrated in the Si core whereas, slot and HPWG facilitate the concentration of modal power in the nano-slot (air).
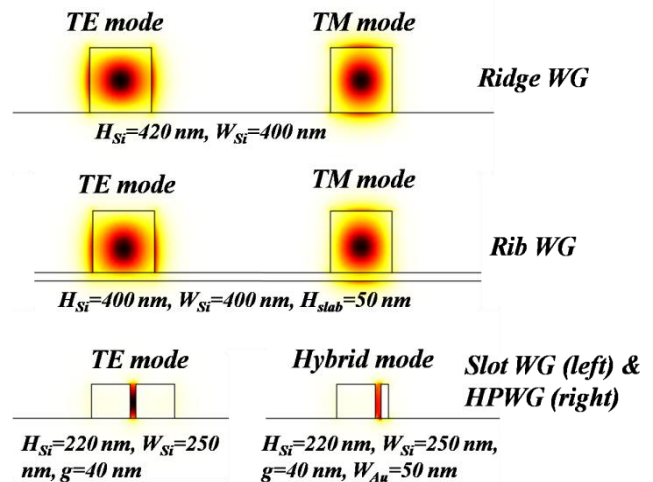

Fig. 2. The E-field intensity arrangement in the ridge (top), rib (middle), slot (bottom left) and HPWG (bottom right) at 1550 nm (color online)

3. Mode sensitivity analysis of optical WGs

For sensing applications, mode sensitivity (S_{mode}) is a vital parameter that should be considered. In this section, we evaluated S_{mode} for the geometric parameters of the WG. S_{mode} is the ratio of the change in effective refractive index and change in ambient refractive index which is expressed as:

$$S_{mode} = \frac{n_{eff2} - n_{eff1}}{n_2 - n_1}$$

where n_{eff2} is the effective refractive index at the refractive index of the analyte (n_2) and n_{eff1} is the effective refractive index at the refractive index of air (n_1). In this analysis, we have used n_2=1.03 for all the four WG schemes.

1) Ridge WG

The mode is guided in the ridge WG when n_{eff} is higher than the cladding and smaller than the core otherwise it will be radiated into the substrate. Moreover, the higher the n_{eff}, the mode will be robustly guided. The dependence of the n_{eff} on the W_{Si} and H_{Si} is calculated for TE_{00} mode as displayed in Fig. 3 (left). The S_{mode} of TE-polarized light is calculated for ridge WG by utilizing eq. (1) is shown in Fig. 3 (right). As W_{Si} increases, the mode confinement in the core increases which makes the n_{eff} of the propagating mode less influenced by the ambient medium. As a result, the S_{mode} decreases with increasing geometric parameters. The highest S_{mode} for TE-polarization is obtained at 0.58 for W_{Si}=300 nm and H_{Si}=240 nm.
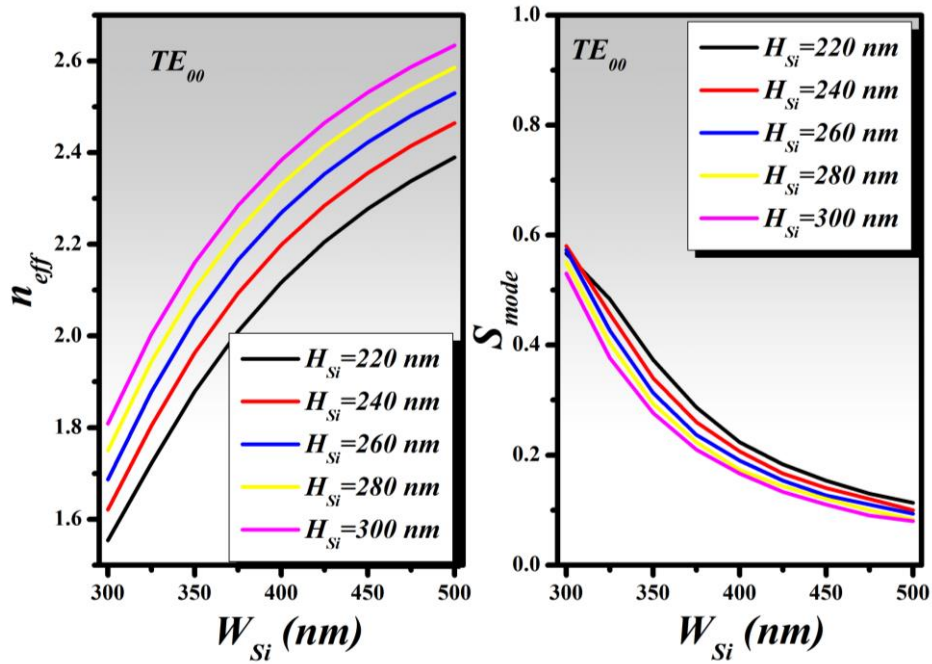

Fig. 3. Effective refractive index (left) and mode sensitivity (right) of ridge WG at TE_{00} polarization (color online)

Most WGs are capable of supporting modes of two independent polarizations. The difference between n_{eff} of the fundamental quasi-TE and quasi-TM modes should be big. This will help in avoiding the coupling between the modes which results due to the variation in mode profiles and the phase mismatch. The n_{eff} of the ridge WG at TM-polarization increases as H_{Si} increases due to the increased mode confinement in the Si core. From Fig. 2, it can be seen that the E-field distribution of the mode is vertically oriented with the evanescent field extending on top of the core while the other part is lost in the substrate. This limits the light-matter interaction from only one side and reduces the S_{mode} for TM-polarization as shown in Fig. 4. The highest S_{mode} of 0.34 is obtained for W_{Si}=400 nm and H_{Si}=245 nm.
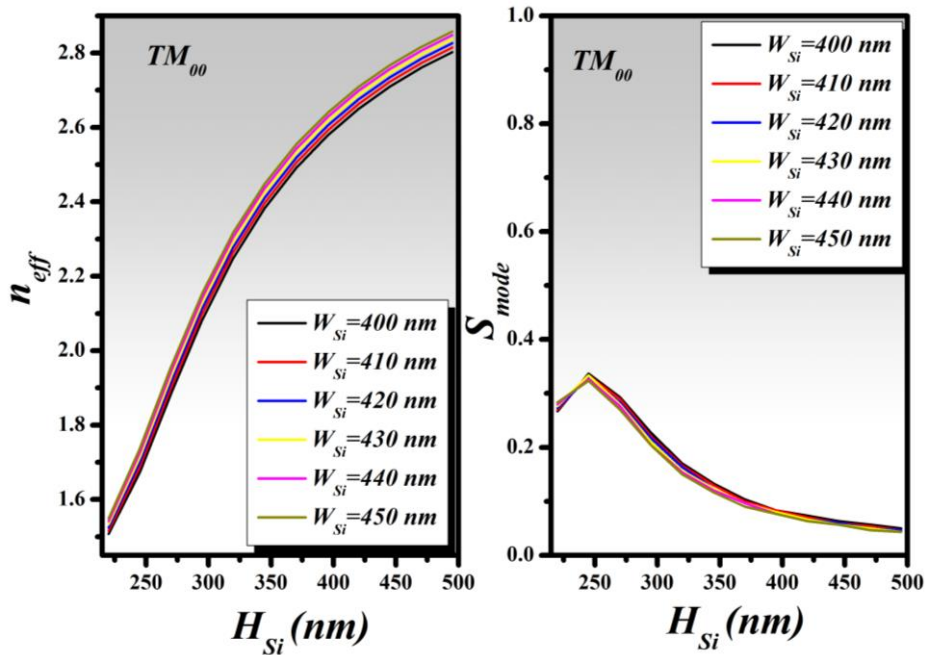
Fig. 4. Effective refractive index (left) and mode sensitivity (right) of ridge WG at TM00 polarization (color online)

2) Rib WG

The rib WG has a thin layer of slab between the core and substrate which elevates the n_{eff} of the TM mode compared to ridge WG. The dependence of n_{eff} concerning H_{slab} is plotted for TE and TM polarizations. It can be seen in Fig. 5 (left) that n_{eff} increases with geometric parameters of the WG providing better mode confinement in the core

which significantly affects the S_{mode} as shown in Fig. 5 (right). The highest S_{mode} for TE and TM polarizations is obtained at 0.36 and 0.14, respectively. The results suggest that this WG geometry is highly unattractive for sensing applications where robust interaction between light and matter is needed.
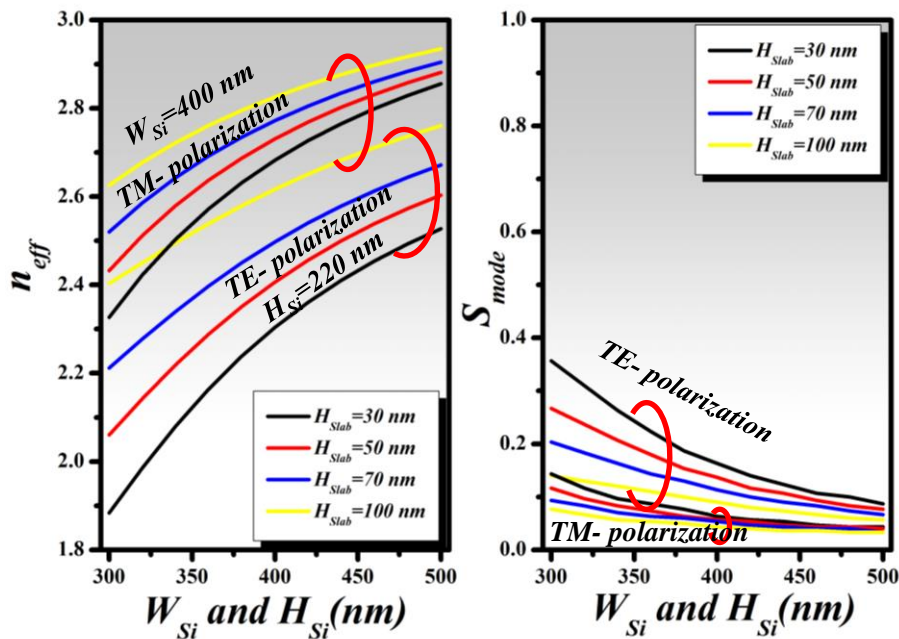

Fig. 5. Effective refractive index (left) and mode sensitivity (right) of rib WG. The W_{Si} is fixed at 400 nm for TM-mode analysis whereas H_{Si} is fixed at 220 nm for TE-mode analysis (color online)

3) Slot WG

The dependence of n_{eff} of slot WG at TE polarization is studied by varying g and W_{Si} at a constant H_{Si}=220 nm as shown in Fig. 6 (left). Conversely, this WG scheme is unable to confine the quasi-TM mode as the E-field remain constant at the interface. The n_{eff} of the slot WG start increasing with an increasing W_{Si} and approaches to the n_{eff} of ridge and rib WG schemes as shown in Fig. 6 (left). This is because large W_{Si} allows the confinement of mode in the Si rails which reduces the mode power in the nano-slot as shown in Fig. 6 (right). At optimized WG parameters such as W_{Si}=250 nm and g=40 nm, the highest S_{mode} of 0.8 is obtained which drops significantly to 0.18 as W_{Si} approaches 500 nm as shown in Fig. 6 (middle).

In comparison to other traditional WGs, slot WG can provide high field confinement in the slot which in general not possible to attain. This characteristic makes slot WG an attractive candidate for applications that require strong interaction of light with matter such as sensing and nonlinear photonics [28].
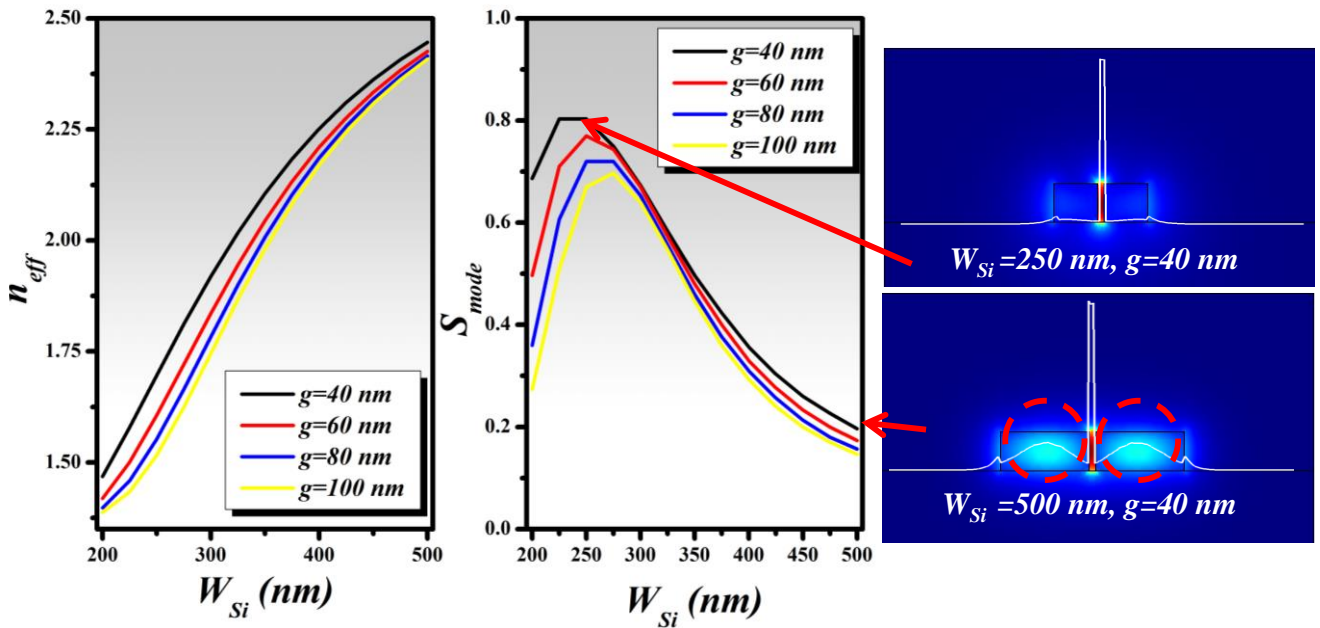

Fig. 6. Effective refractive index (left) and mode sensitivity (middle) of slot WG. The H_{Si} is fixed at 220 nm. The E-field distribution in the slot WG (right) (color online)

4) HPWG

The real part of n_{eff} of the hybrid mode is calculated by varying g, W_{Au} and W_{Si} as demonstrated in Fig. 7 (left). W_{Si} has a stronghold on n_{eff} of the hybrid mode which increases significantly as W_{Si} increases. The E-field distribution of HP mode is shown in the inset of Fig. 7 (right). At optimized geometric parameters such as g=40 nm, W_{Au}=30 nm and W_{Si}=230 nm, the S_{mode}= 0.97 is attained which shows the strength of hybrid mode in nano-slot and its response to the ambient medium as presented in Fig. 7 (middle). S_{mode} diminishes as W_{Si} approaches 400 nm, this is because the mode power starts shifting to Si rail as indicated by a red dotted circle in Fig. 7 (right).
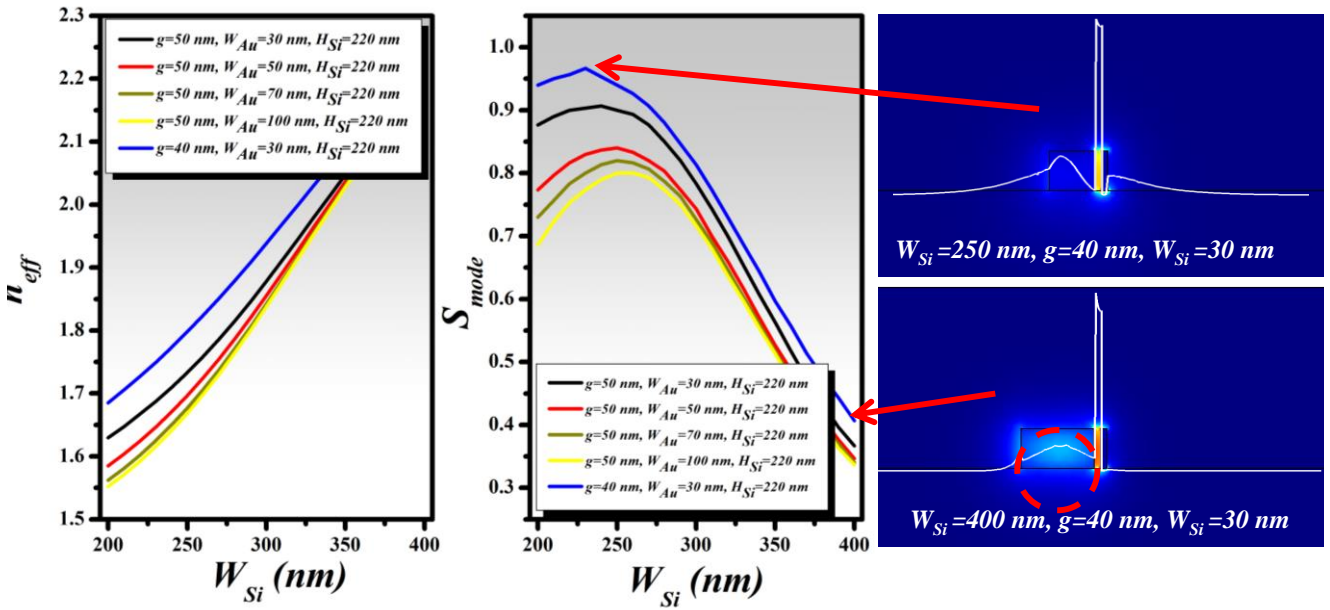
Fig. 7. Effective refractive index (left) and mode sensitivity (middle) of HPWG. The HSi is fixed at 220 nm.
The E-field distribution in the HPWG (right) (color online)

HPWG integrates the characteristics of the dielectric and plasmonic WGs [25]. The excitation of surface electron fluctuation in the HPWG focuses on the photons to reside near the metal surface. This helps in the reduction of radiation loss. The high optical confinement offered by this WG scheme is beyond the diffraction limit. While the propagation loss is comparatively low as compared to Si slot WG. Si photonics has turned out to be very interesting due to its fabrication compatibility with the regular CMOS microelectronics technology [29]. For that reason, it is exciting to realize a Si-based HPWG with basic fabrication processes.

4. Evanescent field ratio analysis of optical waveguides

The sensitivity of the optical WGs is directly related to the occurrence of an evanescent field in the upper cladding. The evanescent field ratio (EFR) is employed to study the performance of the optical sensors that are formed on the phenomena of evanescent field interaction with the matter. The sensors with extraordinary EFR can have strong interaction with the ambient medium,

accordingly, the sensitivity is enhanced. EFR can be calculated as the ratio of intensity integration of upper cladding to the overall intensity integration in the WG and is expressed as [30, 31]:

$$\text{EFR} = \frac{\iint_{\text{Upper cladding}} |E(x, y, z)|^2 dxdydz}{\iint_{\text{total}} |E(x, y, z)|^2 dxdydz}$$

In the case of slot and HPWG, the mode is confined in the low index nano-slot (g), therefore the intensity integration of the upper cladding of these WG is the sum of energy in the nano-slot and energy above the WG. By utilizing eq. (2), the EFR of ridge, rib, slot and HPWG is determined concerning the geometric parameters. Fig. 8a and Fig. 8b presents the variation in EFR of ridge WG for TE and TM polarizations which deteriorates as W_{Si} and H_{Si} increases, respectively. The TE mode has relatively higher EFR compared to TM mode which agrees with the S_{mode} analysis of rib WG as presented in Fig. 8 c.
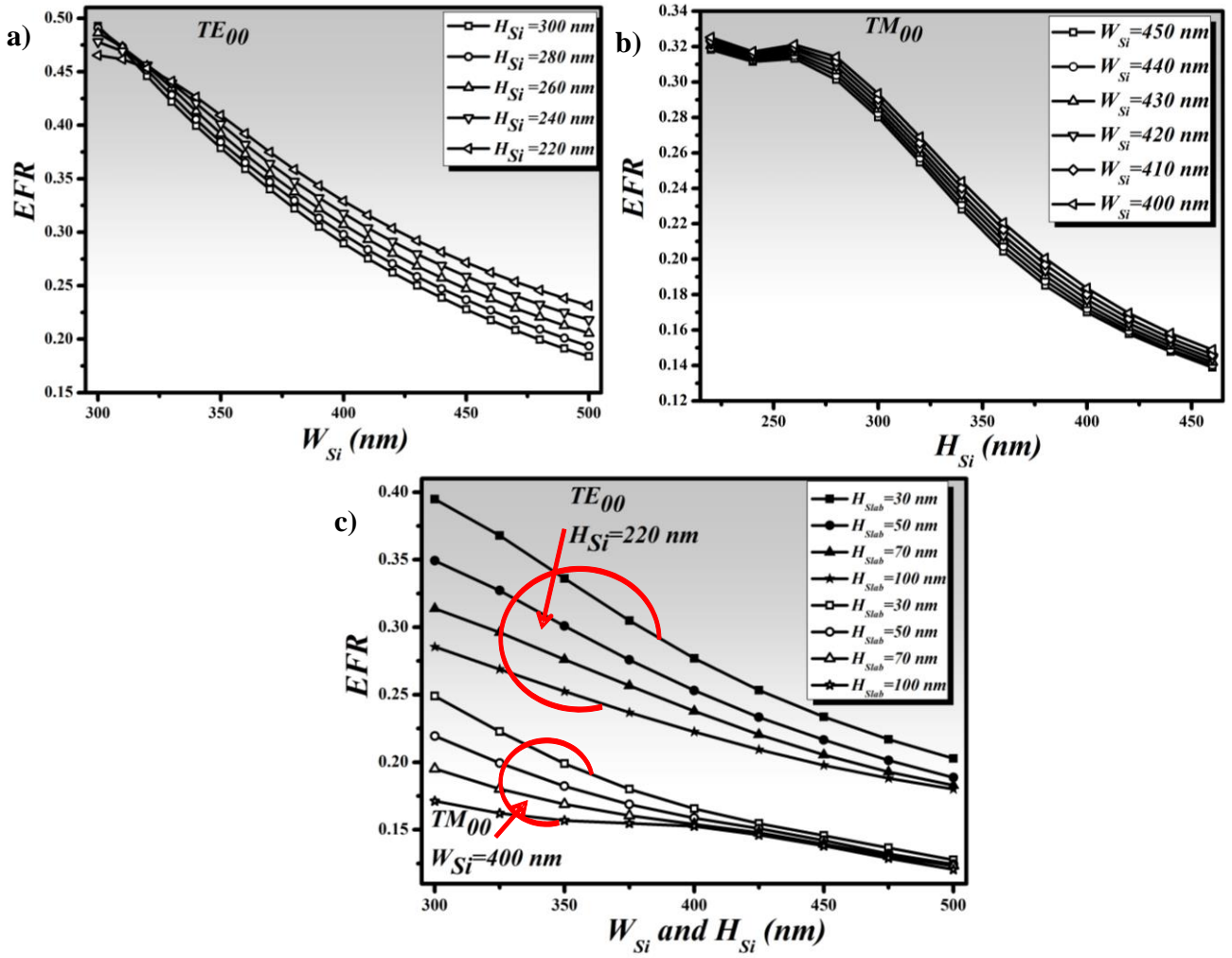
Fig. 8. EFR calculation for a) Ridge WG at TE polarization, b) Ridge WG at TM polarization,
c) Rib WG at TE and TM polarized light (color online)

The EFR analysis of slot and HPWG is presented in Fig. 9 which shows the highest value of ~0.69 for both the WGs that can be obtained by optimizing the WG geometry. This value is relatively higher than the ridge and rib WGs. For that reason, slot and HPWGs are highly attractive for sensing applications.
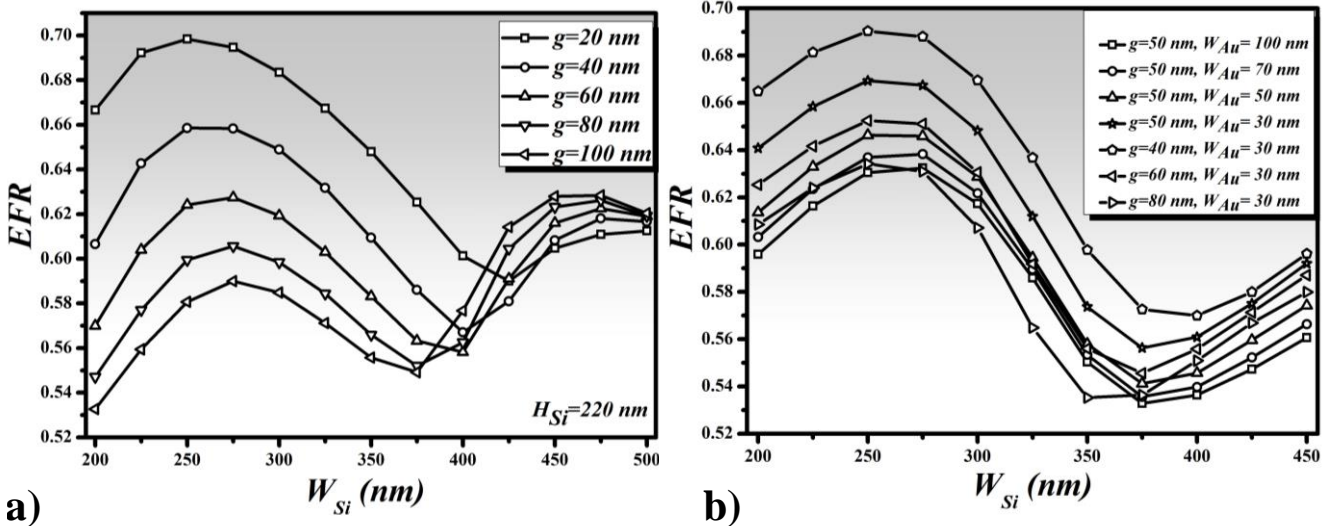

Fig. 9. EFR calculation for a) Slot WG, b) HPWG

5. Propagation loss calculation

Propagation loss results due to the scattering of energy from propagating to radiation modes. This happens due to the WG sidewalls roughness and also direct loss due to material absorption or the leakage of light into the substrate if the optical field is not adequately guided [32]. Here, we are considering the propagation loss which arises due to the geometric parameters of the WG which are not able to fully confine the mode in the core. The variation in propagation loss is determined by varying different geometric parameters depending on the WG type. And loss is calculated by using the formula:

$$\text{Loss} \left(\frac{dB}{\mu m} \right) = \frac{10 \text{xlog} \frac{P_{out}}{P_{in}}}{\text{Propagation length}}$$

where Pin and Pout are the power at the input and output of the WG, respectively. The total propagation length of the WG is fixed at 3 μm. Conventional WGs such as ridge and rib can be modelled and fabricated with optimized parameters such that their propagation loss is as low as 0.07 dB/μm and 0.4 dB/μm, respectively at the cost of low S_{mode} and EFR as shown in Fig. 10 a, b.
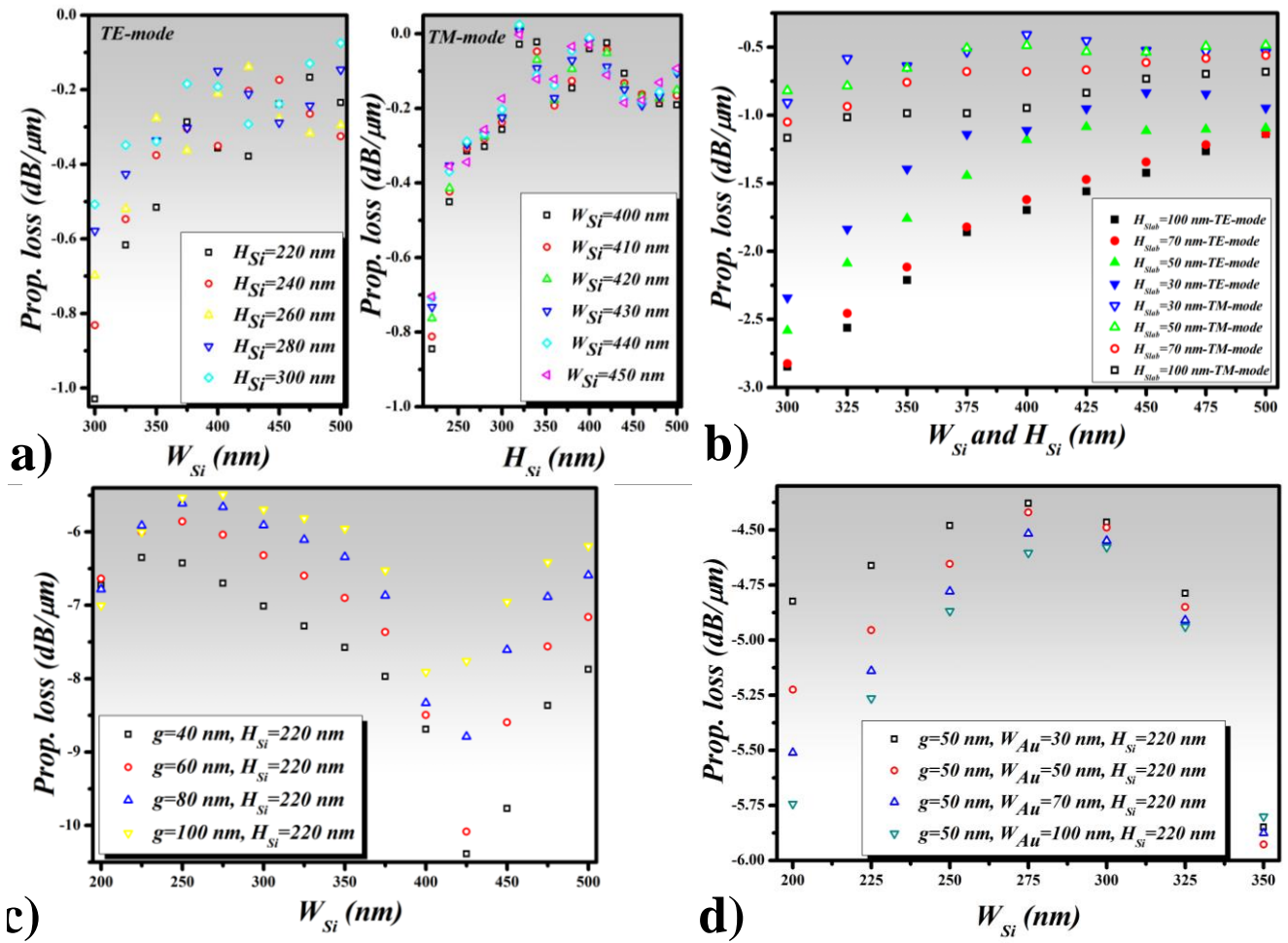

Fig. 10. a) Propagation loss of ridge WG at a) TE and TM mode, b) Propagation loss of Rib WG at TE and TM mode, c) Propagation loss of slot WG, d) Propagation loss of HPWG (color online)

The main constraint of slot and HPWGs is their high transmission loss. As shown in Fig. 10, these WGs have high propagation loss as compared to the conventional WG structures [33]. HPWG has lower propagation loss compared to slot WG thanks to the marriage of standard WG and plasmonic WG. Moreover, in slot WG, the light is better confined in the slot region, any surface roughness, appear during the manufacturing procedure can cause major scattering loss. Consequently, the realization of low-loss slot WG is a difficult task. If both these WGs are designed for their highest S_{mode} and EFR, then propagation loss of 5.53 dB/μm and 4.48 dB/μm is obtained for slot and HPWG, respectively as presented in Fig. 10 (c, d).

6. Sensing application

Here, we studied the sensing capabilities of ridge WG, slot WG and HPWG based on the wavelength interrogation method. We are not considering rib WG in this analysis due to its low S_{mode} and EFR as calculated in previous sections. The measurement of changes in λ_{res} is the widely used interrogation method in ring resonators (RRs) [34]. The sensors used to detect refractive index (hereafter represented as RI) variations reveal several applications related to biological and chemical and have been widely investigated in recent times. For instance, the concentration and pH value of an unknown solution can be assessed based on the alteration of the RI [35, 36]. A biosensing semiconductor nanowire RI sensor with a sensitivity of 235 nm/RIU is demonstrated [37]. A long-period fiber grating sensor is proposed for RI sensing applications [38]. The highest sensitivity of 135 nm/RIU for quasi-TM ring resonators was experimentally demonstrated [39]. Nevertheless, the bulk sensitivity of 270 nm/RIU has been presented by optimizing the WG thickness [40]. For a resonator based on strip WG, this value is 90% of the maximum realizable sensitivity. Lately, an extremely responsive photonic sensor based on porous silicon RR has

been proposed which offers a sensitivity of 439 nm/RIU for low RI variations [41].

In this work, micro-RR designs are modelled based on ridge, slot and HPWG structures as shown in Fig. 11 (a-c). The geometric parameters of the three designs are similar to provide a comparative study on the sensor performance. The device design has a height (H_{Si}) = 220 nm while the gap (G) between the bus WG and ring is fixed at 100 nm. The RR has a radius R which is maintained at 1500 nm (from the outer edge) which is similar for all three designs. The width of WG used in the ridge WG and HPWG RR is denoted as W_a which is varied between 300-350 nm. For the HPWG resonator, the Si circular ridge WG encircling an Au disk in the center. While for slot WG, W_o and W_i denote the outer and inner WG width, respectively which are varied to increase the confinement in the slot area. The variation in width takes place in the following combinations: ((W_o=350 nm and W_i=250 nm), (W_o=340 nm and W_i=260 nm), (W_o=330 nm and W_i=270 nm), (W_o=320 nm and W_i=280 nm), (W_o=310 nm and W_i=290 nm), (W_o=300 nm and W_i=300 nm)). The slot width (g) = 40 nm is used in slot WG and HPWG which is air (n=1.0). Fig. 11 (d-e) presents the E-field confinement of a ridge, slot and HPWG RR at their respective λ_{res}.
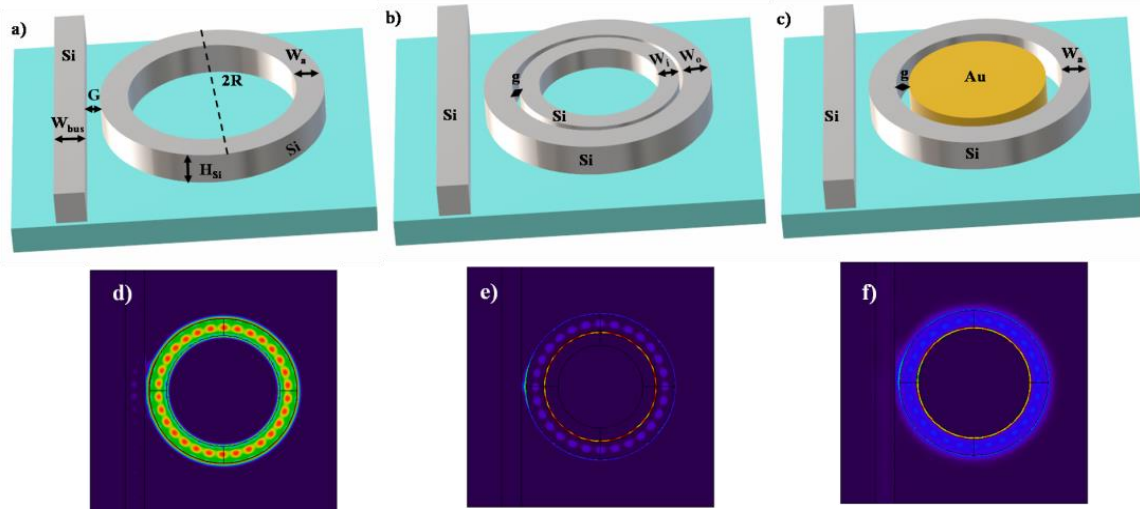

Fig. 11. Schematic representation of RR based on, a) Ridge WG, b) Slot WG, c) HPWG, d) E-field distribution of mode at λ_{res} in ridge WG RR, where W_a=350 nm, e) E-field distribution of mode at λ_{res} in slot WG RR where W_o=350 nm and W_i=250 nm and g=40 nm, f) E-field distribution of mode at λ_{res} in HPWG RR where W_o= 340 nm, g=40 nm (color online)

To attain the spectral characteristics of the proposed sensor devices, the ambient medium is loaded with a dielectric material of n=1.03 for all three sensor designs. The transmission spectrum and E-field distribution are simulated via a 2D-FEM. S_{mode} and EFR analysis of slot and HPWG suggest that RRs based on these WGs can provide strong light-matter interaction as compared to a ridge WG RR having the same geometric parameters [42, 43]. High sensitivity is always desirable in refractive index sensors, which strongly depends on light polarization, optical loss

and the light-matter interaction. Sensitivity can be calculated as S=$\Delta\lambda/\Delta n$, where $\Delta\lambda$ represents the shift of the sensor resonance in nm and Δn is the difference of the RI in the medium. Along with the sensitivity, the figure of merit (FOM), which is expressed as S/FWHM is another important parameter that should also be taken into consideration while designing the RR sensor.

In Fig. 12 (a, b), the S and FOM of RRs are plotted for the width of WG for Δn = 0.03. The HPWG RR delivers maximum S in comparison with the other two designs at

W=300 nm (where W= W_o and W_a for slot and ridge/HPWG, respectively) which deteriorates as W increases as shown in Fig. 12a. The S_{max} of RR based on HPWG reduces from 333.33 nm/RIU to 170 nm/RIU when W varies from 300 nm to 350 nm. The RR based on slot WG has the lowest FWHM =2.66 nm at W=350 nm whereas RR based on ridge WG has wide FWHM=6.65 nm at W=300 nm. Therefore, a sensor composed of Slot WG offers higher FOM as compared to the other two sensor configurations as shown in Fig. 12 b.
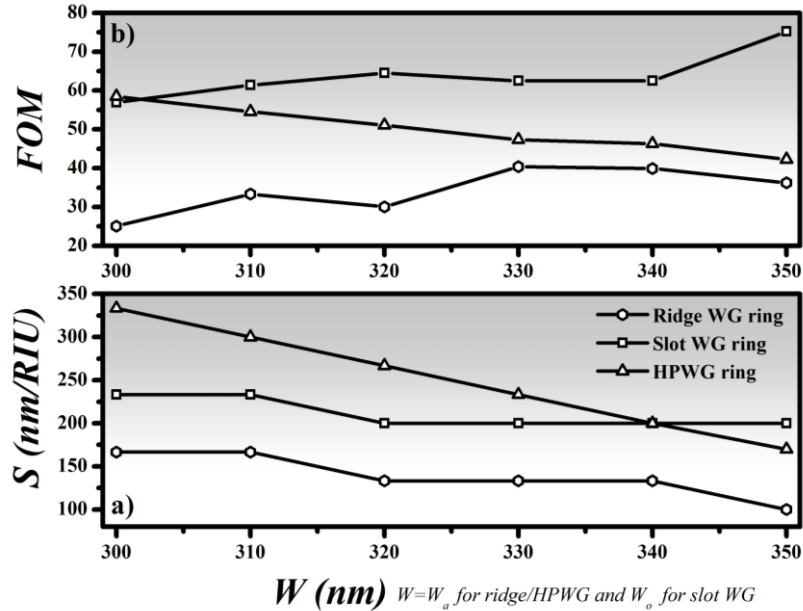

Fig. 12. a) Sensitivity, b) FOM of ridge WG ring, slot WG ring and HPWG ring

Although the HPWG RR has the maximum S, however, its wide FWHM is responsible for lowering down its FOM than slot WG RR. Previously described, FOM is expressed as the fraction between S and FWHM, hence, RR having small FWHM offers a superior FOM as demonstrated in Fig. 12 b. The FOM_{max} is approximately 75.2, 58.5 and 40.4 for slot WG, HPWG and ridge WG RR, respectively. The spectral characteristics of the RR designs are tabulated in Table 1.

Table 1. Spectral characteristics of RRs based on ridge, slot and HPWG

Type	Ridge WG RR	Slot WG RR	HPWG RR
S_{max} (nm/RIU)	167	233.3	333.3
FWHM (nm) at W=350 nm	2.76	2.66	4.02
FOM_{max}	49.9	75.18	58.5

7. Proposed fabrication steps in silicon photonics

SOI is the most attractive platform used in microelectronics and micro-mechanics. It is not merely utilized as a passive substrate but can also be used as active material in electronic or mechanical components. To start with, a hard mask (thin metal layer, for instance, Ti or Cr) is deposited on the SOI substrate followed by a spin coating of positive photoresist. The lithographic process is used to pattern the photoresist which facilitates the removal of the unwanted hard mask using wet chemical etching. Subsequently, the photoresist is removed via a developer and the necessary patterning can be obtained via the wet-chemical etching process. Crystalline Si can be etched by using a strong aqueous alkaline media such as NaOH, KOH or TMAH-solutions via

$$Si + 2OH + 2H_2O \rightarrow Si(OH)_4 + H_2 \rightarrow SiO_2(OH)_2^2 + 2H_2$$
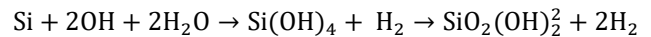
Optical elements with sub-100 nm features have turned out to be important for sophisticated research and development in optics, electronics and material science applications. Si high-resolution gratings are effectively established via inductively coupled plasma (ICP) dry etching with precise substrate temperature management [44]. The detailed fabrication process of silicon WGs can be found in [45-47].

8. Concluding remarks

In this work, we studied the mode sensitivity and evanescent field ratio of a silicon ridge WG, rib WG, slot WG and HPWG. These WGs are the basic building block of

integrated optics. Depending on their mode sensitivity and evanescent field ratio, these WGs can be employed in sensing applications where high interaction between light and matter is preferred. Numerical analysis has shown that slot WG and HPWG show their dominance over a ridge and rib WG in terms of mode sensitivity (0.8 for slot WG and 0.97 for HPWG) and evanescent field ratio (~0.69). However, due to the highly sensitive mode, these WGs suffer from high optical loss compared to standard silicon WGs. The RR realized on HPWG structure offers the sensitivity of 333.3 nm/RIU which is significantly higher than the RRs based on ridge and slot WGs. However, special care should be taken while designing or fabricating sensor devices such as RRs based on this WG scheme. Fabrication inaccuracy of a few nanometers can lead to high optical loss and low sensitivity. We consider that the results presented in this paper will provide a standard to choose a suitable WG structure for optical interconnects and sensor devices. In the final remarks, we can say that slot and HPWGs are ideal candidate for highly sensitive devices but these cannot be used as long-distance propagation WGs.

Acknowledgements

References

[1] N. L. Kazanskiy, M. A. Butt, S. N. Khonina, Optics and Laser Technology **138**, 106863 (2021).

[2] S. N. Khonina, M. A. Butt, N. L. Kazanskiy, J. Opt. **23**, 065102 (2021).

[3] H. Sohn, Refractive Index of Porous Silicon, Handbook of Porous Silicon, Canham L. (eds) Handbook of Porous Silicon, Springer, Cham. doi.org/10.1007/978-3-319-05744-6_25 (2014).

[4] S. Bondarenko, C. Villringer, P. Steglich, Appl. Sci. **9**, 89 (2019).

[5] R. Nagarajan, C. Doerr, F. Kish, Optical Fiber Telecommunications- Components and Subsystems (Sixth Edition): Chapter 2-Semiconductor Photonic Integrated Circuit Transmitters and Receivers, 2013: 25-98. ISBN: 978-0-12-396958-3. DOI. org/10.1016/C2011-0-06843-6.

[6] M. A. Butt, S. N. Khonina, N. L. Kazanskiy, Laser Physics **29**(7), 076202 (2019).

[7] M. R. Billah et al., Optica **5**(7), 876 (2018).

[8] J. E. Bowers, H. Park, Y-H. Kuo, A. W. Fang, R. Jones, M. J. Paniccia, O. Cohen, O. Raday, Research and Applications, 8-11 July Salt Lake City, Utah United States. doi.org/10.1364/IPNRA.2007.ITuG1 (2007).

[9] K. Shibuya, Y. Atsumi, T. Yoshida, Y. Sakakibara, M. Mori, A. Sawa, Optics Express **27**(4), 4147 (2019).

[10] M. A. Butt, S. N. Khonina, N. L. Kazanskiy, Laser Physics **28**(11), 116202 (2018).

[11] M. A. Butt, S. N. Khonina, N. L. Kazanskiy, Laser Physics **29**(4), 046207 (2019).

[12] K. J. Miller, K. A. Hallman, R. F. Haglund, S. M. Weiss, Optics Express **25**(22), 26527 (2017).

[13] M. A. Butt, S. N. Khonina, N. L. Kazanskiy, Journal of Modern Optics **66**, 1172 (2019).

[14] N. L. Kazanskiy, S. N. Khonina, M. A. Butt, Sensors **20**, 3416 (2020).

[15] M. A. Butt, S. N. Khonina, N. L. Kazanskiy, Applied Optics **59**(26), 7821 (2020).

[16] O. Powell, Journal of Lightwave Technology **20**(10), 1851 (2020).

[17] W. Wei, X. Yan, B. Shen, J. Qin, X. Zhang, Nanoscale Res Lett. **13**, 227 (2018).

[18] C. A. Barrios, K. B. Gylfason, B. Sanchez, A. Griol, H. Sohlstrom, M. Holgado, R. Casquel, Optics Letters **32**(21), 3080 (2007).

[19] S. P. Chan, C. E. Png, S. T. Lim, G. T. Reed, V. M. N. Passaro, J. Lightw. Technol. **23**(6), 2103 (2005).

[20] R. A. Soref, J. Schmidtchen, K. Petermann, IEEE Journal of Quantum Electronics **27**(8), 1971 (1991).

[21] M. A. Butt, A. N. K. Reddy, S. N. Khonina, Computer Optics **42**(2), 244 (2018).

[22] V. R. Almeida, Q. Xu, C. A. Barrios, M. Lipson, Opt. Lett. **29**, 1209 (2004).

[23] T. Baehr-Jones et al., Appl. Phys. Lett. **92**(16), 163303 (2008).

[24] J. Xiao, J. Liu, Z. Zheng, Y. Bian, G. Wang, J. Opt. **13**, 105001 (2011).

[25] M. A. Butt, S. N. Khonina, N. L. Kazanskiy, Journal of Modern Optics **65**(9), 1135 (2018).

[26] M. A. Butt, N. L. Kazanskiy, S. N. Khonina, Laser Phys. **30**, 016202 (2020).

[27] M. Z. Alam, J. S. Aitchison, M. Mojahedi, IEEE Journal of Selected Topics in Quantum Electronics **19**(3), 4602008 (2013).

[28] M. A. Butt, S. N. Khonina, N. L. Kazanskiy, Journal of Modern Optics **65**(2), 174 (2018).

[29] J. T. Kim, IEEE Photonics Technology Letters **23**(4), 206 (2010).

[30] M. A. Butt, S. N. Khonina, Optik **168**, 692 (2018).

[31] M. A. Butt, S. A. Degtyarev, S. N. Khonina, N. L. Kazanskiy, Journal of Modern Optics **64**(18), 1892 (2017).

[32] I. Papakonstantinou, K. Wang, D. R. Selviah, F. A.

Fernandez, Optics Express **15**(2), 669 (2007).

[33] J. R. Ong, V. H. Chen, Optics Express **23**(26), 33622 (2015).

[34] M. A. Butt, S. N. Khonina, N. L. Kazanskiy, Laser Physics **29**(4), 046208 (2019).

[35] P. Vaiano et al., Laser Photon. Rev. **10**(6), 922 (2016).

[36] T. Guo, J. Lightw. Technol. **35**(16), 3323 (2017).

[37] Y. L. Wang et al., ACS Photon. **4**(3), 688 (2017).

[38] C. Teng, F. Yu, Y. Ding, J. Zheng, Proc. SPIE, 10231: Art. no. 102311M (2017).

[39] D.-X. Xu et al., Opt. Express **18**(2), 22867 (2010).

[40] S. Talebifard et al., Biomed. Opt. Express **8**(2), 500 (2017).

[41] R. Caroselli et al., Optics Express **25**(25), 31651 (2017).

[42] S. N. Khonina, N. L. Kazanskiy, M. A. Butt, IEEE Sensors Journal **20**(15), 8469 (2020).

[43] M. A. Butt, N. L. Kazanskiy, S. N. Khonina, IEEE Sensors Journal **20**(17), 9779 (2020).

[44] A. L. Goodyear, S. Mackenzie, D. L. Olynick, E. H. Anderson, J. Vac. Sci. Technol. B. **18**(6), 3471 (2000).

[45] M. Loncar, T. Doll, J. Vuckovic, A. Scherer, Journal of Lightwave Technology **18**(10), 1402 (2000).

[46] M. J. Shaw, J. Guo, G. A. Vawter, S. Habermehl, C. T. Sullivan, Fabrication techniques for low-loss silicon nitride WGs, Proc. SPIE 5720, Micromachining Technology for Micro-Optics and Nano-Optics III, (22 January 2005); http://doi.org/10.1117/12.588828.

[47] G. T. Reed, P. Y. Yang, W. R. Headley, P. M. Waugh, G. Z. Mashanovich, D. Thomson, R. M. Gwilliam, Proc. SPIE 6477, Silicon Photonics II, 64770E (9 February 2007); http://doi.org/10.1117/12.705180.

_____

*Corresponding author: butt.m@ssau.ru